SUPPPOTING INFORMATION

Direct Observation of Chemical Origins in Crystalline $(Ni_xCo_{1-x})_2B$ Oxygen Evolution Electrocatalysts

Xinzhi Ma[ab], Kaixin Zhao[b], Yu Sun[a], Yue Wang[a], Feng Yan[a], Xitian Zhang[b]*, and Yujin Chen[a]*

1 College of Physics and Optoelectronic Engineering, Harbin Engineering University, Harbin 150001, China.
E-mail: chenyujin@hrbeu.edu.cn
2 Key Laboratory for Photonic and Electronic Bandgap Materials, Harbin Normal University, Harbin 150025, China.
E-mail: xtzhangzhang@hotmail.com

Keywords: Chemical origin, Binary metal catalysts, Crystalline CoNiB, and OER.

Experiments

Chemicals. Cobalt (purity, >99.99%; diameter, ~0.5 μm), Nickel (purity, >99.99%; diameter, ~0.5 μm) boron powder (purity, >99.9%) were purchased from Aladdin Chemical Co., Ltd. Hydrophilic and hydrophobic carbon papers were purchased from Toray Co., Ltd. It is worth noting that the potassium hydroxide aqueous solution was further purified as the electrolyte.

Experimental Methods. All purchased materials were used without further treatment. The synthesis of high-performance materials was mainly through a ball-milled method. The mixing mole ratio of metal and B is 1:1 for both Ni_2B and Co_2B. For bimetal $(Ni_xCo_{1-x})_2B$ materials, the mixing mole ratio ($R_{Ni}/R_{Co}/B$) are 0.25:0.75:1, 0.50:0.50:1 and 0.75:0.25:1, respectively. All the samples were ball-milled using a planetary ball mill (Fritsch Pulverisette 4) with the ball-to-power weight ratio of 20:1. An Ar (99.99%) inflation−deflation process was employed to remove the air in the grinding bowls, and the pressure of bowls was vacuumed to 95 KPa. Rotational speeds and reaction time were of 900 rpm and 10 h for all samples.

Structure Characterizations. XRD data were collected on a Rigaku D/max-2600/PC with Cu Kα radiation (λ = 1.5418 Å). The morphology and size of samples were characterized by a scanning electron microscope (Hitachi SU70) and an FEI Tecnai-F20 transmission electron microscope equipped with a Gatan imaging filter (GIF). XPS analyses were carried out by using a spectrometer with Mg Kα radiation (PHI 5700 ESCA System). The binding energy was calibrated with the C 1s position of contaminant carbon in the vacuum chamber of the XPS instrument (284.6 eV).

Electrochemical Measurements. Electrochemical measurements of individual electrodes were conducted on a VMP3 electrochemical workstation (Bio Logic) with a standard three-electrode electrochemical system using $(Ni_xCo_{1-x})_2B$ catalysts on hydrophilic carbon paper as the working electrode; a graphite rod and an Ag/AgCl electrode were used as the counter and the reference electrodes, respectively. The carbon paper working electrode was prepared as described below: the catalysts were mixed with (conductive agent) carbon nanotubes and dispersed in N-methyl-2-pyrrolidone solvent containing 7.5 wt % PVDF under sonication, in which the weight ratio ($W_{catalyst}/W_{CNT}/W_{PVDF}$) was 8/1/1. Then the slurry was coated onto a piece of carbon paper, on which the loading density of the catalyst was about 0.6 mg cm^{-2}. The as-prepared catalyst film was vacuum-dried at 90 °C. Electrochemical measurements of the catalysts were measured in 1 M KOH solution after purging the electrolyte with N_2 gas for 30 min. For each catalyst, CV curves were first recorded from 0 to 0.8 V vs Ag/AgCl at a scan rate of 2 mV s^{-1}. The activation of catalysts was carried out under a potential range from 0 V to that corresponding to 100 mA cm^{-2} for several cycles until the curves remained unchanged. Then, the activity of the catalysts toward the OER was evaluated by cycling CV from 0 to 0.7 V vs Ag/AgCl at a scan rate of 2 mV s^{-1}. The long-term stability test was carried out by cycling CV measurements for 1000 times at a scan rate of 50 mV s^{-1}. All potentials measured were calibrated to RHE using the following equation: $E_{(RHE)} = E_{(Ag/AgCl)} + 0.21\ V + 0.059 \times pH$. All current densities presented are corrected against 95% compensated Ohmic potential drop. The preparation of hydrophobic carbon paper was same as that of hydrophilic one, instead changing hydrophilic carbon paper with a hydrophobic one.

TOF Calculation. The number of active sites (n) was first examined by employing cyclic voltammograms with phosphate buffer (pH 7) at a scan rate of 50 mV s^{-1}. Then the number of the voltammetric charges (Q) could be determined after deduction of the blank value. The number of moles (n) could be determined with the equation n

(mol) = Q/4F, where F is Faraday's constant. TOF (s^{-1}) could be calculated with the equation TOF (s^{-1}) = I/4nAF, where I (A) was the current of the polarization curve obtained by CV measurements and A is the geometric area of the electrodes.

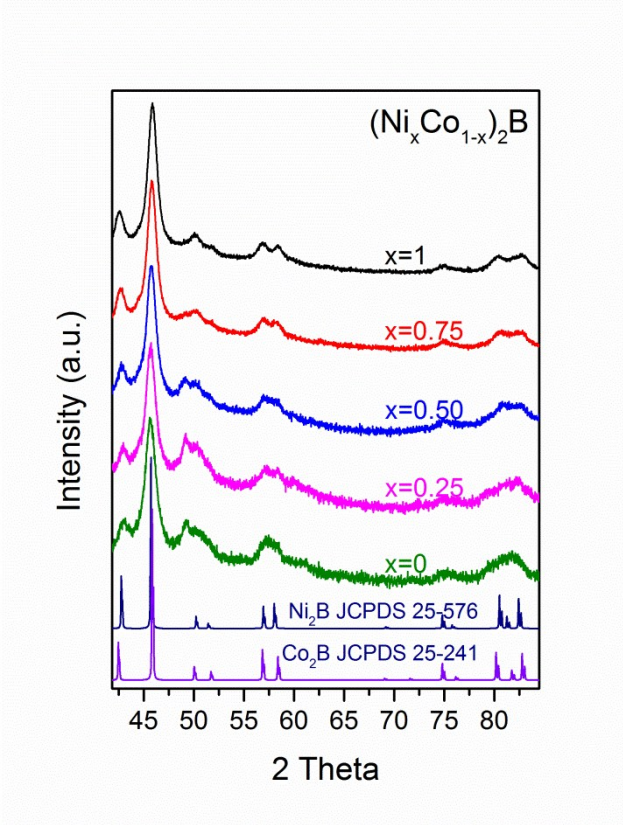

Figure S1 XRD pattern of this series of $(Ni_xCo_{1-x})_2B$ catalysts, respectively.

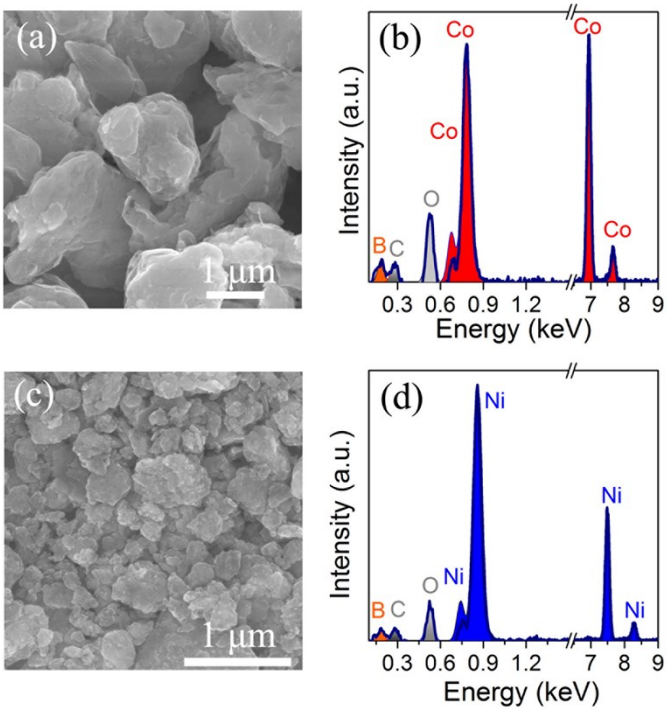

Figure S2 a) and c) SEM of Co_2B and Ni_2B, respectively; b) and d) EDX data of Co_2B and Ni_2B, respectively.

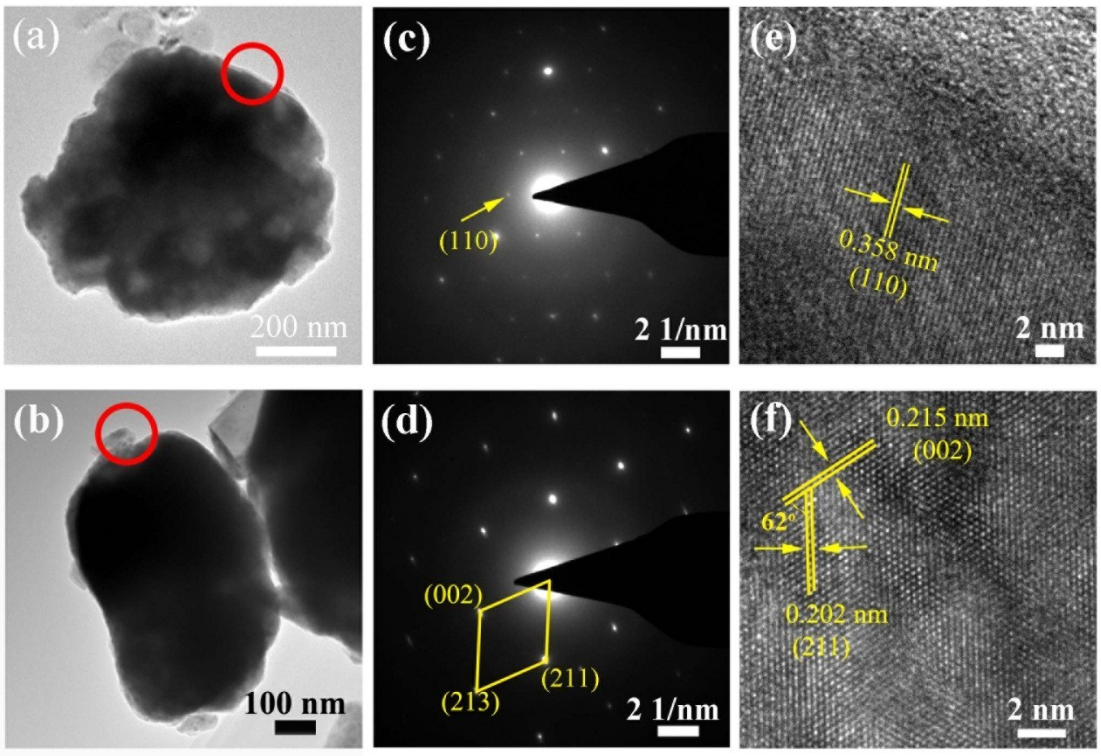

Figure S3 Structural characterizations of Ni_2B and Co_2B samples. a) and b) TEM patterns; c) and d) HRTEM patterns; e) and f) SAED images.

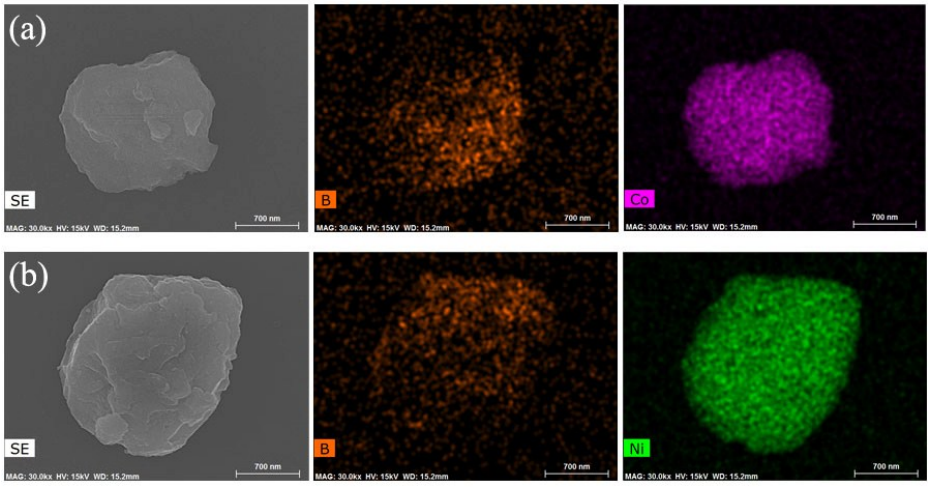

Figure S4 a) and b) Elemental mapping images of Co_2B and Ni_2B

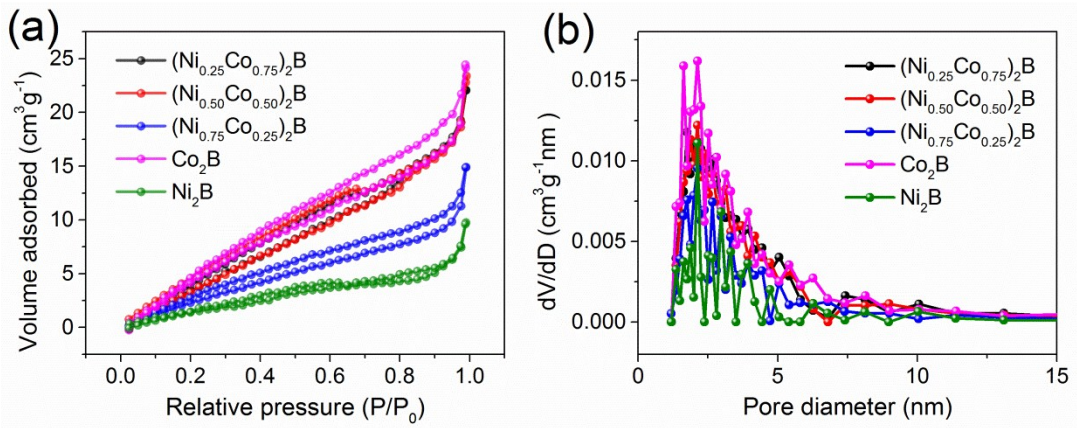

Figure S5 (a, b) N_2 adsorption-desorption isotherm and the corresponding pore-size distribution of these materials.

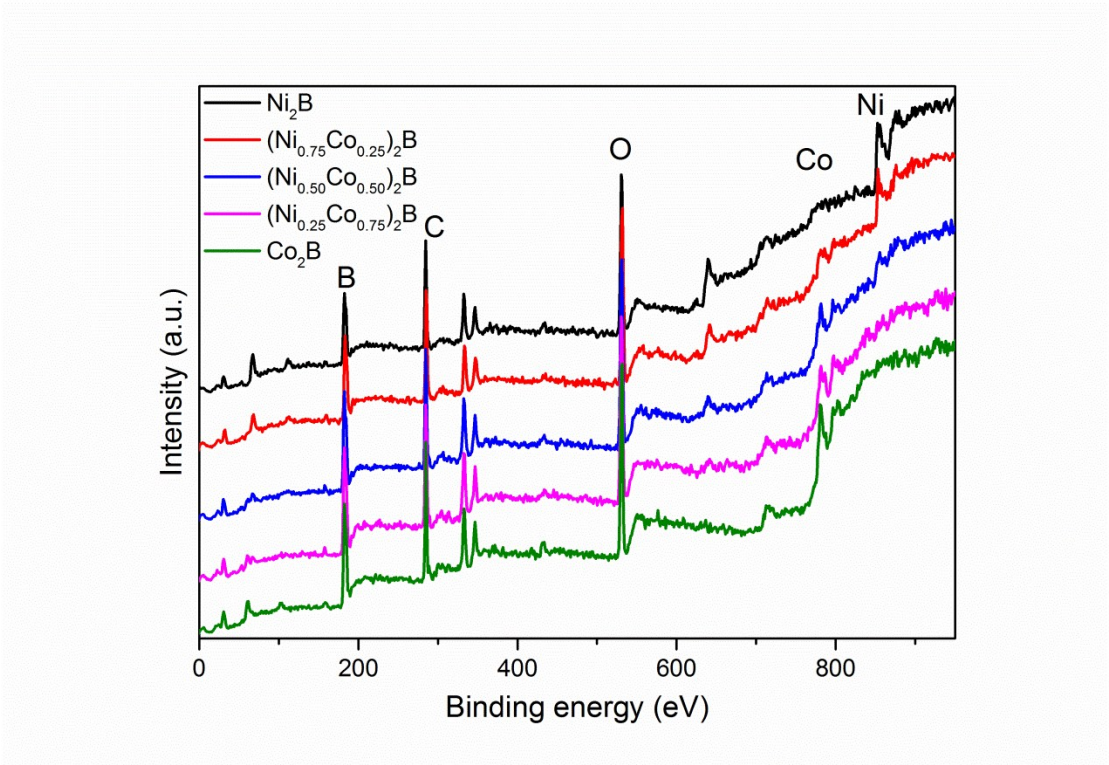

Figure S6 Survey XPS spectrums of this series of samples.

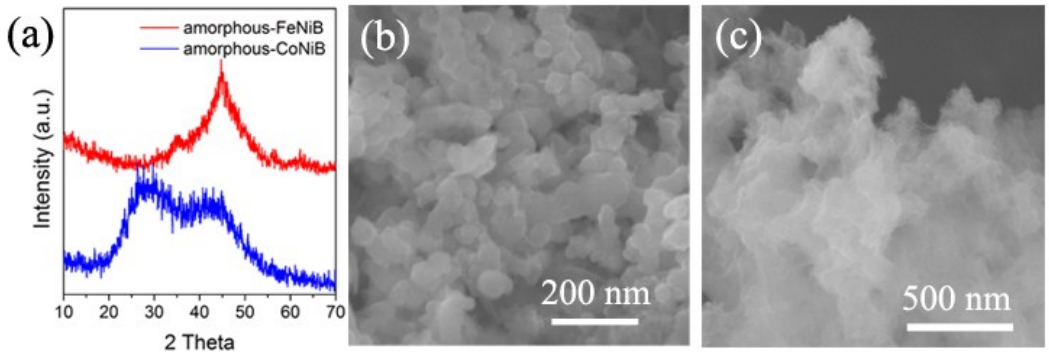

Figure S7 a) XRD patterns of amorphous FeNiB and CoNiB, respectively. b) and c) SEM images of amorphous FeNiB and CoNiB, respectively.

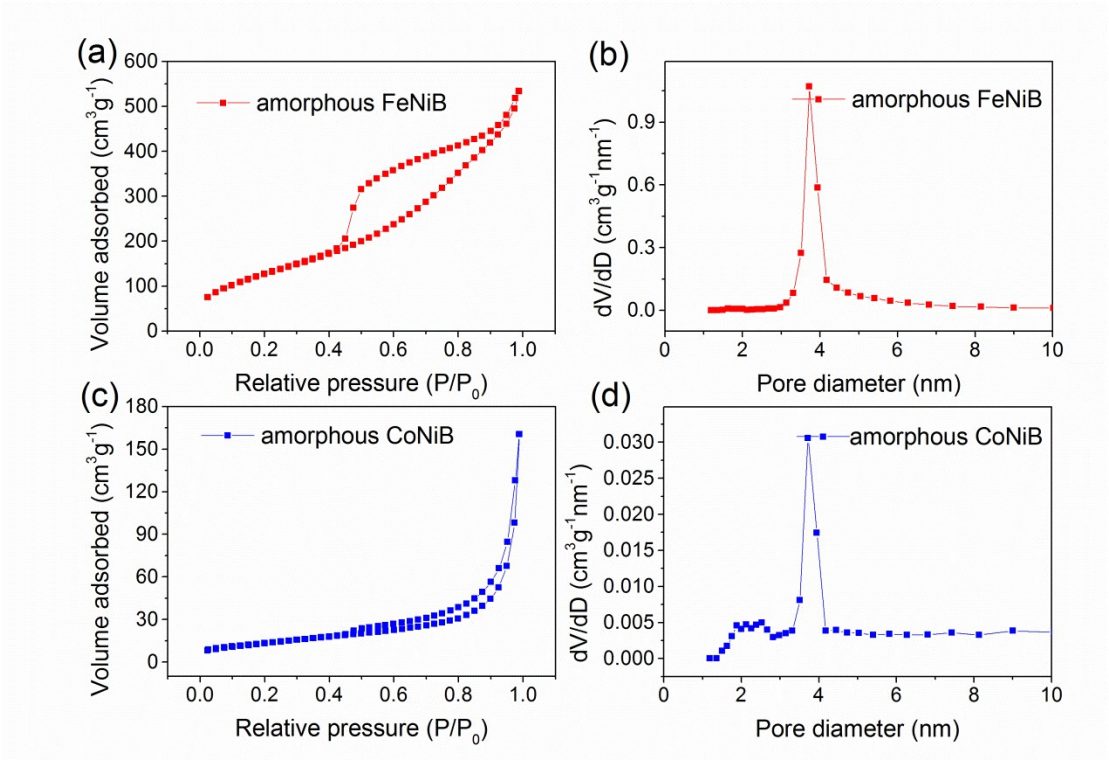

Figure S8 (a, c) N_2 adsorption-desorption isotherm of amorphous FeNiB and CoNiB; (b, d) and Their corresponding pore-size distribution.

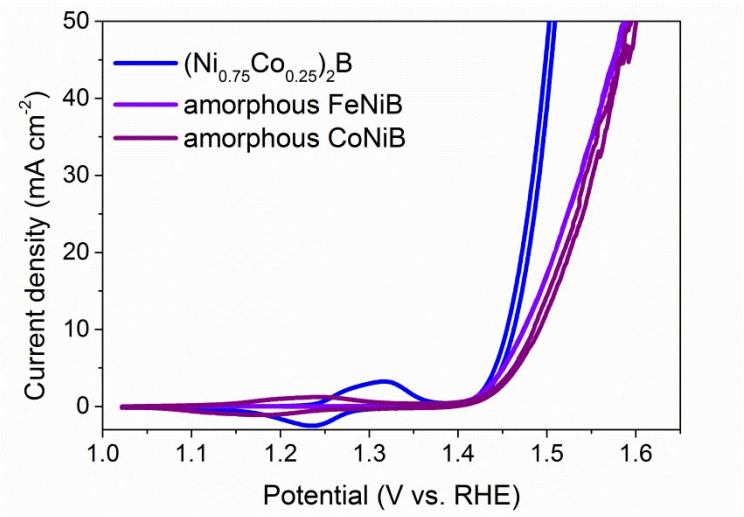

Figure S9 CV curves of crystal $(Ni_{75}Co_{25})_2B$, amorphous FeNiB and amorphous CoNiB, respectively.

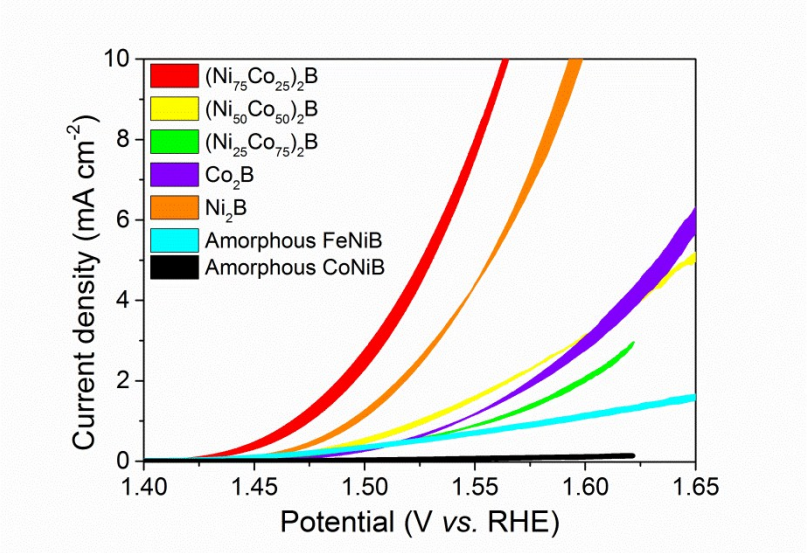

Figure S10 Normalized surface area CV curves of this series of crystal catalysts, amorphous FeNiB and amorphous CoNiB.

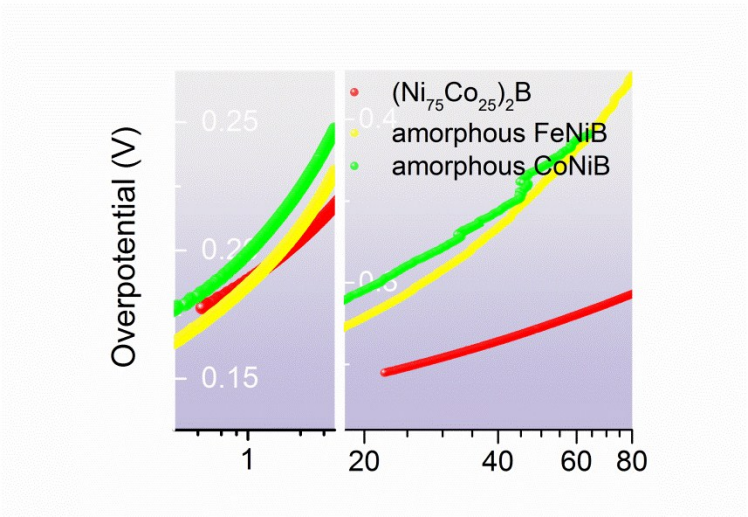

Figure S11 Tafel slopes of crystal $(Ni_{75}Co_{25})_2B$, amorphous FeNiB and amorphous CoNiB, respectively.

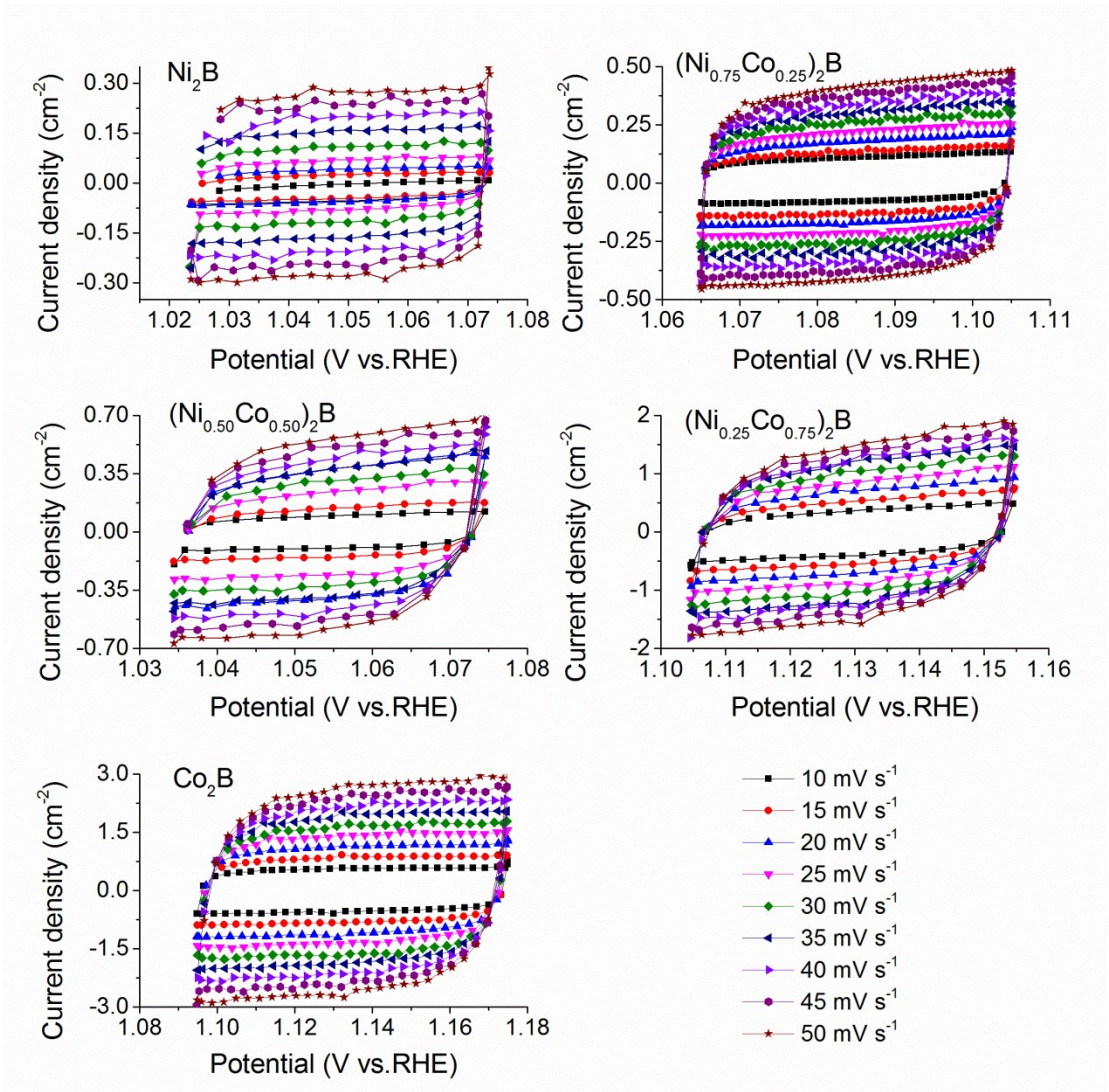

Figure S12 C_{dl} of this series of catalysts.

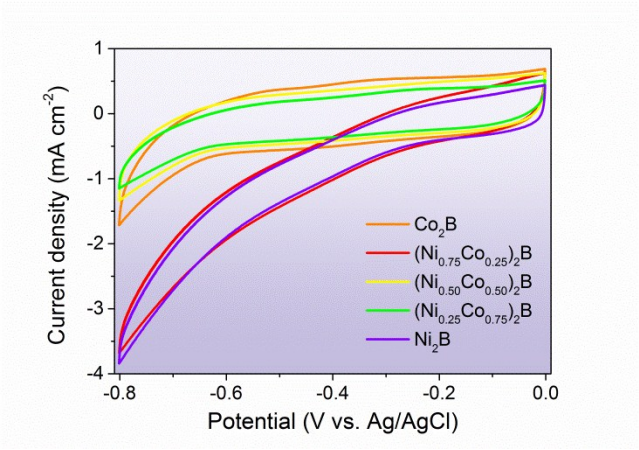

Figure S13 Cyclic voltammetry cycling in pH = 7 phosphate buffer with a scan rate of 50 mV s^{-1} range from - 0.8 to 0 V vs. Ag/AgCl of this series of catalysts.

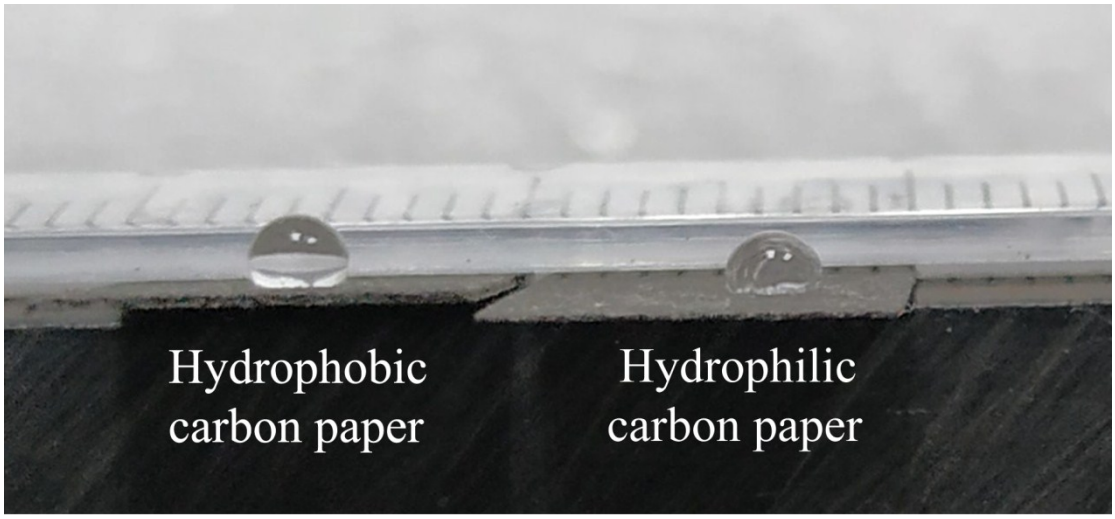

Figure S14 Droplets of 10 µL deionized water on hydrophobic and hydrophilic carbon papers after 5 minutes air exposition.
This picture indicates that water droplet is more easy and quick to adsorb on hydrophilic carbon paper.

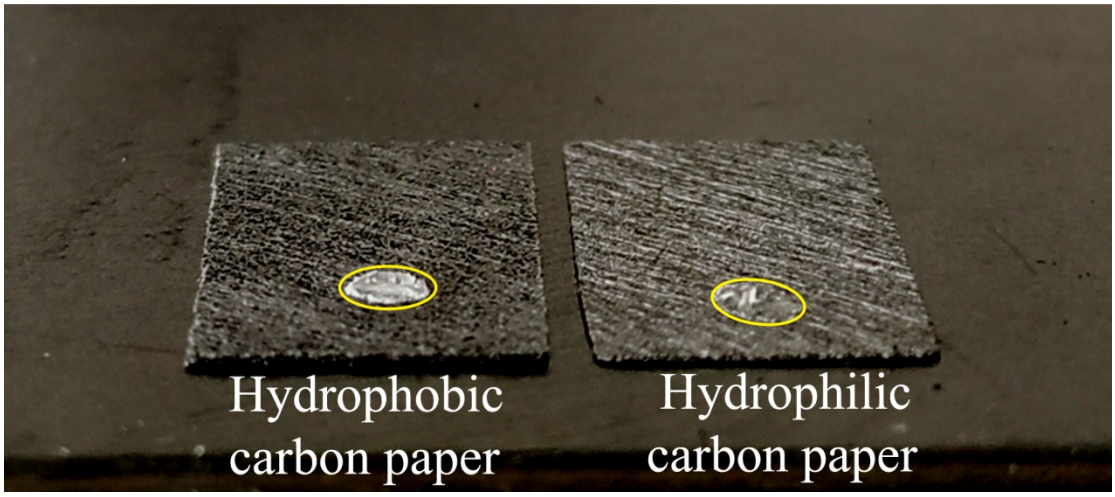

Figure S15 Droplets of 10 µL 1M KOH solution on hydrophobic and hydrophilic carbon papers after 12 hours air exposition.

This picture indicates that KOH solution is easier and more tend to contact with hydrophilic carbon papers.

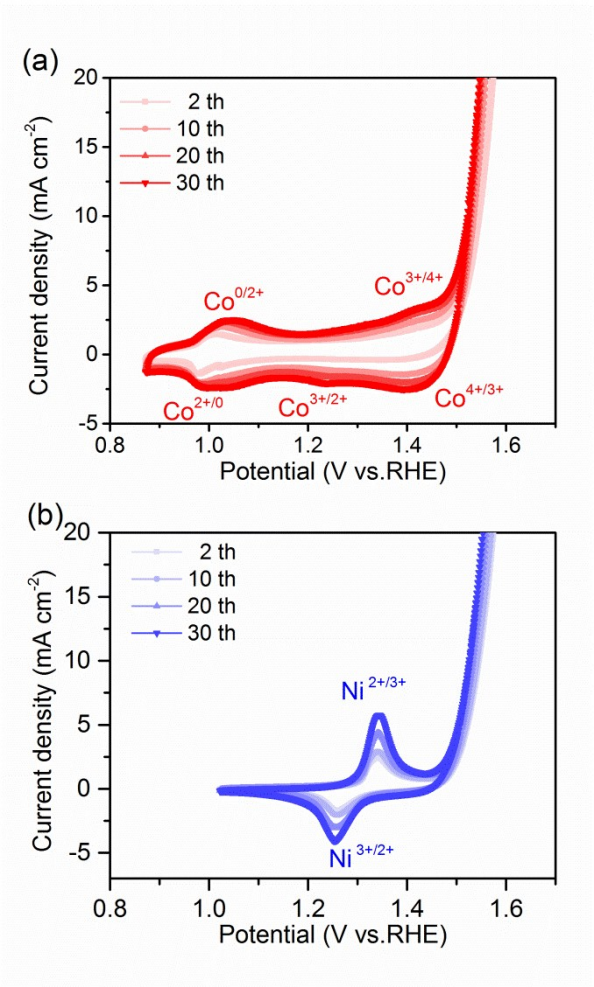

Figure S16 a) and b) CV curves of Co_2B, Ni_2B loading on hydrophilic papers and measured at 50 mV s^{-1} in 1M KOH solutions, respectively.

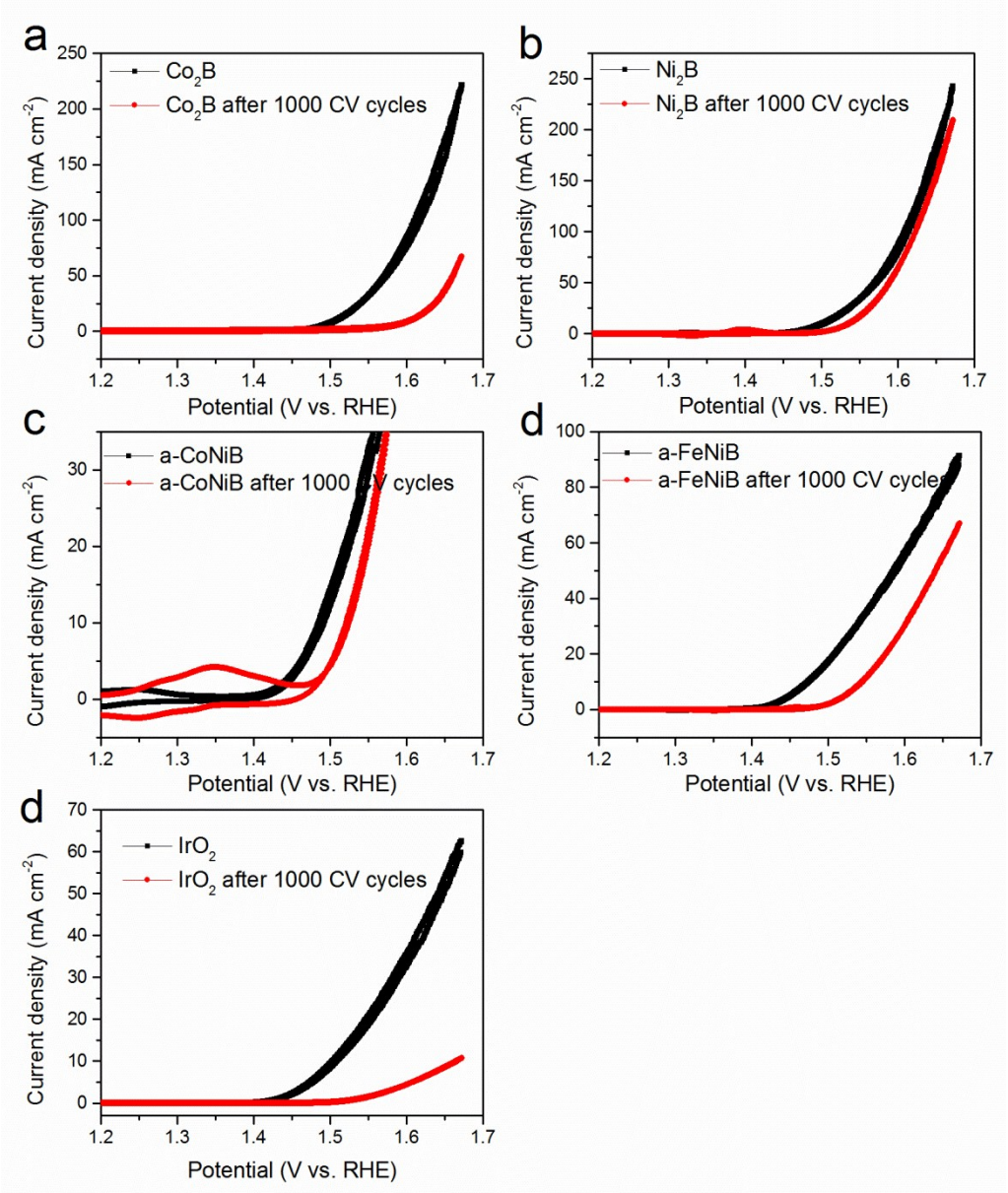

Figure S17 Stabilities of Co_2B, Ni_2B, amorphous CoNiB, amorphous FeNiB, and IrO_2 catalysts.

Table S1. Comparison of OER activity of the crystal $(Ni_{0.75}Co_{0.25})_2B$ catalyst with recently reported bimetal OER catalyst measured in 1M KOH solutions.

Catalysts	Tafel slope (mV dec^{-1})	$\eta_{10mA\ cm^{-2}}$ (mV)	References
$(Ni_{0.75}Co_{0.25})_2B$ nanoparticles	**34.5**	**224**	**This work**
Macroporous CoFeP TPAs/Ni	42	198	J. Mater. Chem. A, 2019, 7, 17529.[14]
FeNiP−NP	76	180	Adv. Mater., 2017, 29, 1704075.[16]
CoFe-MOF	44	265	ACS Catal., 2019, 9, 7356−7364.[18]
N-CoFe LDHs /NF	40.03	233	Adv. Funct. Mater., 2018, 28, 1703363.[22]
NiCo-LDHs@B_2O_3/CP	61	213	ACS Sustainable Chem. Eng., 2018, 6, 14257−14263. [24]
a-ternary Ni-Co-B	113	300	Electrochimica Acta, 2019, 296, 644e652. [27]
NiCoFeB nanochains	46	284	Small, 2019, 15, 1804212. [28]
Co_2–Fe–B	62.6	298	ACS Nano, 2014, 8, 3970-3978. [41]
Hierarchical $Ni_{0.69}Co_{0.31}$–P yolk–shell spheres	81	266	Nanoscale, 2016, 8, 19129-19138. [43]
Ni–Mo nitride nanotubes	94	295	J. Mater. Chem. A, 2017, 5, 13648. [44]
NiCo-LDHs nanoplates	40	367	Nano Lett., 2015; 15, 1421-1427.
$FeNi_3N$/NG	45.3	$\eta 20$=258	J. Mater. Chem. A, 2019,7, 1083-1091
CoPh/NG	54	$\eta 20$=300	Nanoscale, 2016, 8, 10902-10907.
NiFeB	43	$\eta 10$=251	Nano Research, 2018, 11, 1664-1675.23.
$NiCo_2S_4$/CC	89	$\eta 20$=280	Nanoscale, 2015, 7, 15122-15126.
TiN@Ni_3N nanowire arrays	93.7	$\eta 10$=350	J. Mater. Chem. A, 2016, 4, 5713-5718.
NiCoP-NWAs/NF	116	$\eta 20$=270	J. Mater. Chem. A, 2017, 5, 14828-14837.
Zn-Co-S/TM	79	$\eta 20$=330	Electrochimica Acta, 2016, 190, 360-364.
NiMoN-550	94	$\eta 20$=321	J. Mater. Chem. A, 2017, 5, 13648-13658.
$NiCo_2S_4$ NW/GDF	47	$\eta 20$=308	Small, 2017, 13, 1700936.
Fe-Ni hydroxide/GMC	57	320	ChemSusChem, 2016, 9, 1-9.
α-$Co_4Fe(OH)_x$	53	295	J. Mater. Chem. A, 2017, 5,1078
Co-Fe-P-1.7	58	260	ACS Appl. Mater. Interfaces, 2017, 9, 362-

			370.
Exfoliated NiCo LDHs	41	330	Nature communications, 2014, 5:4477.
Exfoliated CoCo LDHs	45	350	Nature communications, 2014, 5:4477.
Exfoliated NiFe LDHs	40	300	Nature communications, 2014, 5:4477.
Exfoliated CoNi LDHs/CP	40	367	Nano Lett., 2015, 15, 1421-1427.
$CoFeNiO_X$/NF	-	240	J. Am. Chem. Soc., 2016, 138, 8946-8957.
MnCoOP particles	52	320	Angew. Chem. Int. Ed, 2017, 56, 2386-2389.

Table S2. Peak intensity informations of Co^{3+}-O and Ni^{3+}-O species in Raman spectra of bimetal catalysts after OER measurements.

Catalysts	Peak intensity of Co^{3+}-O (counts)	Peak intensity of Ni^{3+}-O (counts)	Average peak intensity of active oxygen (counts)	Peak intensity ratio of Co^{3+}-O/ Ni^{3+}-O (%)	Peak intensity ratio of active oxygen/ Ni^{3+}-O (%)
$(Ni_{0.75}Co_{0.25})_2B$	937.87	988.84	896.26	95.4	90.6
$(Ni_{0.50}Co_{0.50})_2B$	644.76	681.35	570.41	94.6	83.7
$(Ni_{0.25}Co_{0.75})_2B$	352.84	464.02	211.82	76.0	46.6

Table S3. Normalized content of surface Co^{2+}, Co^{3+}, Ni^{2+} and Ni^{3+} related species of bimetal catalysts after OER measurements.

Catalysts	Normalized surface Co^{2+} content (%)	Normalized surface Co^{3+} content (%)	Normalized surface Ni^{2+} content (%)	Normalized surface Ni^{3+} content (%)
$(Ni_{0.75}Co_{0.25})_2B$	44.5	55.5	73.4	26.6
$(Ni_{0.50}Co_{0.50})_2B$	40.4	59.6	55.8	44.2
$(Ni_{0.25}Co_{0.75})_2B$	54.8	45.2	44.7	55.3